Molecular Pharmacology Fast Forward. Published on June 7, 2019 as DOI: 10.1124/mol.119.116640
This article has not been copyedited and formatted. The final version may differ from this version.

The L46P mutant confers a novel allosteric mechanism of resistance towards the influenza A virus M2 S31N proton channel blockers

Rami Musharrafieh,[‖,†] Panagiotis I. Lagarias,[‡] *Chunlong Ma,*[‖] *Gene S. Tan,*[#,§] *Antonios Kolocouris,*[‡,*] *Jun Wang*[‖,*]

[‖]Department of Pharmacology and Toxicology, College of Pharmacy, The University of Arizona, Tucson, USA

†Department of Chemistry and Biochemistry, The University of Arizona, Tucson, AZ, USA

‡Department of Pharmaceutical Chemistry, Faculty of Pharmacy, National and Kapodistrian University of Athens, Panepistimiopolis-Zografou 15771, Greece

[#]J. Craig Venter Institute, La Jolla, CA, USA

[§]Department of Medicine, University of California, San Diego, La Jolla, CA 92037

*Corresponding authors

Molecular Pharmacology Fast Forward. Published on June 7, 2019 as DOI: 10.1124/mol.119.116640
This article has not been copyedited and formatted. The final version may differ from this version.

Running Title Page

Running title: An allosteric mutant against the AM2 S31N proton channel

*Corresponding authors: Drs. Antonios Kolocouris and Jun Wang.

Dr. Antonios Kolocouris contact info:

Address: National and Kapodistrian University of Athens, Panepistimiopolis-Zografou 15771, Greece

Email: ankol@pharm.uoa.gr

Dr. Jun Wang contact info:

Address: 1657 E. Helen St, BIO5 Room 303, Tucson, AZ, 85721, United States.

Phone: 520-626-1366

Email: junwang@pharmacy.arizona.edu

Number of text pages:

Number of Tables: 2

Number of Figures: 6

Number of References: 53

Number of words in Abstract: 231

Number of words in Introduction: 739

Number of words in Discussion: 898

List of abbreviations: WT, wild-type; **MD, molecular dynamics;** MM-GBSA, molecular mechanics-generalized born surface area; TM, transmembrane; SPR, structure-property relationship; MDCK, Madin-Darby canine kidney; TEVC, two-electrode voltage clamp.

Molecular Pharmacology Fast Forward. Published on June 7, 2019 as DOI: 10.1124/mol.119.116640
This article has not been copyedited and formatted. The final version may differ from this version.

ABSTRACT

The FDA-approved influenza A antiviral amantadine inhibits the wild-type (WT) AM2 channel but not the S31N mutant predominantly found in circulating strains. In this study, serial viral passages were applied to select resistance against a newly developed isoxazole-conjugated adamantane inhibitor that targets the AM2 S31N channel. This led to the identification of the novel drug-resistant mutation L46P located outside the drug binding site, which suggests an allosteric resistance mechanism. Intriguingly, when the L46P mutant was introduced to AM2 WT, the channel remained sensitive towards amantadine inhibition. To elucidate the molecular mechanism, molecular dynamics (MD) simulations and binding free energy molecular mechanics-generalized born surface area (MM-GBSA) calculations were performed on WT and mutant channels. It was found that the L46P mutation caused a conformational change in the N-terminus of the transmembrane residues 22-31 that ultimately broadened the drug binding site of AM2 S31N inhibitor **4**, which spans residues 26-34, but not of AM2 WT inhibitor amantadine, which spans residues 31-34. The MM-GBSA calculations showed stronger binding stability for **4** in complex with AM2 S31N compared to its complex with AM2 S31N/L46P, and equal binding free energies of amantadine in complex with AM2 WT and AM2 L46P. Overall, these results demonstrate a unique allosteric resistance mechanism towards AM2 S31N channel blockers, and the L46P mutant represents the first experimentally confirmed drug-resistant AM2 mutant that is located outside of the pore where drug binds.

Molecular Pharmacology Fast Forward. Published on June 7, 2019 as DOI: 10.1124/mol.119.116640
This article has not been copyedited and formatted. The final version may differ from this version.

Significance statement

AM2 S31N is a high profile antiviral drug target as more than 95% of current circulating influenza A viruses carry this mutation. Understanding the mechanism of drug resistance is critical in designing the next generation of AM2 S31N channel blockers. Using one of our previously developed AM2 S31N channel blocker as a chemical probe, we, for the first time, identified a novel resistant mutant L46P. The L46P mutant located outside of the drug binding site. It was shown by molecular dynamics simulations that the L46P causes a dilation of drug binding site between residues 22-31, which affects the binding of AM2 S31N channel blockers, but not the AM2 WT inhibitor, amantadine.

Molecular Pharmacology Fast Forward. Published on June 7, 2019 as DOI: 10.1124/mol.119.116640
This article has not been copyedited and formatted. The final version may differ from this version.

INTRODUCTION

AM2 is a proton selective ion channel essential for the replication of influenza A viruses (Pinto et al., 1992; Takeda et al., 2002; Wang et al., 2015). The AM2 channel is a homotetrameric transmembrane protein with 97 residues per monomer. The N-terminal domain (residues 1-23) is largely unstructured with polar residues that help increase the hydration of the pore to facilitate proton conductance (Kwon and Hong, 2016; Ma and Wang, 2018) and for incorporation into virions (Park et al., 1998). The transmembrane (TM) domain (residues 24-43) is required for the formation of a left-handed 4-helix bundle (Cady and Hong, 2008; Stouffer et al., 2008) and for both proton conductance, selectivity (Balannik et al., 2010) as well as drug binding (Ma et al., 2009). In the TM domain, a conserved H37XXXW41 motif forms the selectivity filter and accounts for proton gating. Four histidine side chain imidazole groups at residue 37 point in the pore region of the channel and are protonated sequentially resulting in pH activation and proton selectivity (Acharya et al., 2010; Hu et al., 2010). Tryptophan 41 acts as a gate to help drive unidirectional conductance from N-terminus to C-terminus (Ma et al., 2013; Tang et al., 2002). The remaining residues 44-97 contain a cytoplasmic amphiphilic helix (44-60) that is responsible for virus budding and scission (Chen et al., 2008; Rossman et al., 2010; Schmidt et al., 2013), and a C-terminal tail (61-97) that binds to the viral matrix protein M1 (McCown and Pekosz, 2006).

Amantadine inhibits influenza A virus replication by blocking the AM2 WT channel. The drug binding site was determined to be the pore region between residues 27 and 34 (Cady et al., 2010; Thomaston et al., 2018). This pore blocking model placed the adamantane (**1**) cage near serine 31 with the polar ammonium group facing the histidine 37 tetrad (**Fig 2A**). Clinical use of amantadine was phased out due to prevailing drug resistance among circulating viruses.

Molecular Pharmacology Fast Forward. Published on June 7, 2019 as DOI: 10.1124/mol.119.116640
This article has not been copyedited and formatted. The final version may differ from this version.

Therefore, it is equally important to study the mechanisms of resistance as the mechanisms of action. Standard method of elucidating drug resistance in the laboratory is to generate escape variants by passaging the virus with increasing antiviral selection pressure. For AM2 WT, mutations L26F, V27A, A30T, S31N, and G34E have emerged as a result of amantadine selection (Wang, 2016; Wang et al., 2015). Of note, all these mutations were located in the AM2 pore region at the amantadine drug binding area.

Several isoxazole-conjugated amantadine analogs (**2-6**) have been developed to inhibit the AM2 S31N mutant channel in electrophysiological and in vitro antiviral assays (Li et al., 2017; Wang et al., 2013a; Wang et al., 2018). The drug binding site and mechanism of action of S31N 19inhibitors were determined by both solution and solid-state NMR (**Fig. 2B**) (Wang et al., 2013a; Wu et al., 2014). Interestingly, AM2 S31N inhibitors bind to the AM2 S31N channel with a flipped orientation compared to amantadine in AM2 WT channel: the hydrophobic adamantane cage is located at the hydrophobic pocket created by G34, and the isoxazole interacts with residues V26 and N31 through side-chain hydrophobic interactions and backbone hydrogen bonding, respectively.

The emergence of drug resistance was previously profiled for several potent AM2 S31N inhibitors (Ma et al., 2016; Musharrafieh et al., 2018). The mutations identified were single mutant AM2 S31N/L26I, AM2 S31N/V27I, or the double-mutant AM2 S31N/L26I/A30T. Molecular modeling showed that the V27I and A30T mutants prevent drug binding directly through pore constriction or changes in the polarity of the channel. Residue 26 is located at the helical interface, and the L26I mutation was postulated to change the local structure of the channel, leading to drug resistance.

Molecular Pharmacology Fast Forward. Published on June 7, 2019 as DOI: 10.1124/mol.119.116640
This article has not been copyedited and formatted. The final version may differ from this version.

Compound **4** was recently developed with optimized *in vitro* pharmacokinetic properties based on structure-property relationship (SPR) studies (Wang et al., 2018). To advance this lead compound further, it is critical to understand its mechanism of resistance. As such, in the present work, serial viral passage experiments were performed with compound **4** using the 2009 H1N1 pandemic influenza A virus, A/California/07/2009. The unusual mutant L46P was identified and led to resistance to **4**; Electrophysiological experiments showed that the AM2 S31N/L46P channel is not blocked by compound **4** nor previously developed AM2 S31N inhibitors (**2**, **3**, **5**, and **6**), but remained functional as a proton-selective channel. The resistance mechanism of AM2 S31N/L46P against compound **4** as well as the effect of AM2 L46P on amantadine inhibition was further investigated using molecular dynamics (MD) simulations and MM-GBSA calculations.

MATERIALS AND METHODS

Cell Lines and Viruses. Madin-Darby canine kidney (MDCK) cells were maintained at 37°C in a 5% CO_2 atmosphere using standard cell culture procedures. MDCK cells overexpressing ST6Gal I (MDCK-ST6Gal I) were cultured in the presence of 7.5 μg/ml puromycin. Influenza A virus strain A/California/07/2009 (H1N1) was amplified in MDCK-ST6Gal I and stored at -80°C with 0.5% BSA prior to use.

Antiviral assays. Antiviral experiments were performed using the plaque reduction assay as previously described (Ma et al., 2016; Musharrafieh et al., 2018). Briefly, a confluent monolayer of MDCK-ST6Gal I was infected with ~100-pfu of H1N1 diluted in DMEM with 0.5% BSA. Infection was synchronized at 4°C for around 1h, then transferred to a 37°C incubator for 1h. Infectious media was subsequently removed and cells were washed with PBS. Cells were

Molecular Pharmacology Fast Forward. Published on June 7, 2019 as DOI: 10.1124/mol.119.116640
This article has not been copyedited and formatted. The final version may differ from this version.

overlaid with DMEM, N-acetyl trypsin (2.0 µg/ml) and 1.2% avicel microcrystalline cellulose and incubated until plaque formation became visible after crystal violet staining (around 2 days after infection). The half-maximal effective concentration (EC_{50}) values were calculated by determining the total plaque area in each well using ImageJ software. Serial passage experiments were performed using a viral titer of 0.001 MOI as previously described (Musharrafieh et al., 2018).

M2 Sequencing. The M2 gene from each passage was sequenced by first extracting the viral RNA using QIAamp viral RNA Mini Kit (Qiagen, Hilden, Germany). The purified viral RNA was reverse transcribed, and a PCR reaction using M-specific primers (5′-TAGATATTAAAGATGAGTCTTC-3′ and 5′-CTCTAGCTCTATGTTGACAAAATGACC-3′) was used to amplify the gene segment. The PCR product was run on a 1% agarose gel, extracted, and purified using Wizard SV Gel and PCR Clean-up System (Promega, Madison, WI). M2 was sent to Eton Bioscience, Inc. for sequencing. Whole-genome sequencing of passaged viruses was performed by the J. Craig Venter Institute (La Jolla, California). Briefly, a one-step multisegment reverse-transcription and PCR amplification approach using virus-specific primers was used to generate amplicons (PMID: 19605485). Libraries were generated using sequence independent single primer amplification (PMID: 18179705) (with each sample double-barcoded) and sequenced on an Illumina MiSeq instrument (2 x 300 bp).

Electrophysiological two-electrode voltage clamp (TEVC) assay. Female *Xenopus laevis* frogs were purchased from Nasco (Fort Atkinson, WI). Oocytes harvesting was performed according to protocol approved by University of Arizona IACUC. Electrophysiological measurements were performed using the AM2 gene out of the A/California/07/2009 as previously described (Balannik et al., 2010; Musharrafieh et al., 2018). Briefly, mRNA coding

Molecular Pharmacology Fast Forward. Published on June 7, 2019 as DOI: 10.1124/mol.119.116640
This article has not been copyedited and formatted. The final version may differ from this version.

A/California/07/2009 AM2 and its variants were synthesized via mMessage and mMachine T7 kit (invitrogen) according to manufacturer protocol. 10-50 ng mRNA was injected into each oocyte. 24 to 72h after mRNA injection, electrophysiological TEVC recordings were performed. Oocytes were constantly held at -20mV, current was recorded at various testing condition. The detailed EC_{50} measurement was described in (Jing et al., 2008). At least 8 concentrations covering the EC_{50} value of each compounds were applied in the TEVC recording. At least 3 oocytes were recorded at each concentration. The percent remaining channel current after application of compounds were plotted against compounds concentration with dose-response function in Prizm 5.0.

The AM2 channel specific conductance was measured as described in (Musharrafieh et al., 2018). Briefly, the membrane currents of individual oocytes expressing A/California/07/2009 AM2 or its mutants were first recorded with TEVC electrophysiology technique. 8 to 10 oocytes expressing AM2 or L46P mutant recorded with different current were saved and fixed with 2% paraformaldehyde for 30 min. Fixed whole oocytes were immuno-stained with primary 14C2 (anti-AM2) (gift from Dr. Robert A. Lamb Northwestern University Evanston, IL) monoclonal antibody and secondary Alexa Fluor 546 labeled goat anti-mouse IgG (Molecular Probes, Inc., Medford, OR). A ZOE fluorescent Cell Imager (Bio-Rad) was used to acquire fluorescence images, and about one-half of the surface of each oocyte was imaged. Photoshop was used to quantify the fluorescence intensity by measuring the greyscale value. As a control for the auto fluorescence signal from the yolk, uninjected oocytes were measured. The relative specific activity of AM2 was obtained by taking the slope of the linear regression curve generated from plotting the whole-cell current against the AM2 expression level (detected by immunofluorescence) for each oocyte.

Molecular Pharmacology Fast Forward. Published on June 7, 2019 as DOI: 10.1124/mol.119.116640
This article has not been copyedited and formatted. The final version may differ from this version.

The L46P mutation was introduced using site-directed mutagenesis (QuikChange Site-Directed Mutagenesis Kit (Agilent, Santa Clara, CA)).

Protein preparation - Docking calculations. Structure of (**4)** was built with Schrödinger 2017-1 platform (Schrödinger Release 2018-1: Maestro, Schrödinger, LLC, New York, NY, 2018) and minimized by the conjugate gradient method using the MMFF94 force field (Halgren, 1996) and a distance-dependent dielectric constant of 4.0 until a convergence threshold of 0.0001 kJ mol^{-1} $Å^{-1}$ was reached. The PDB ID 2L0J was used for AM2 WT (22-62) *apo* protein. N- and C-termini of the AM2 WT (22-62) model systems was capped by acetyl and methylamino groups. After applying the protein preparation module of Maestro, (Schrödinger Release 2017-1: Maestro, Schrödinger, LLC, New York, NY, 2017; Maestro, Version 8.5; Schrodinger, Inc.: New York, NY, 2008) all hydrogens of the protein complex were minimized with the AMBER* force field by means of Maestro/Macromodel 9.6 using a distance-dependent dielectric constant of 4.0. The molecular mechanics minimizations were performed with a conjugate gradient (CG) method and a threshold value of 0.0001 kJ $Å^{-1}$ mol^{-1} as the convergence criterion. AM2 S31N (22-62) protein was obtained by manual mutation of S31 to N31. Molecular dynamics (MD) simulations of AM2 S31N (22-62) in hydrated 1-palmitoyl-2-oleoyl-glycero-3-phosphocholine (POPC) for 1 μs produced a well equilibrated *apo* protein AM2 S31N structure. The simulated AM2 S31N (22-62) *apo* protein was superimposed with AM2 S31N (19-49) in complex with compound **2** (M2WJ332) (PDB:2LY0) (Wang et al., 2013a) which after deletion of AM2 S31N (19-49) resulted in complex of AM2 S31N (22-62) with **2**. The structures of the protein AM2 S31N (22-62) and ligand **2** were saved separately and were used for the subsequent docking calculations of ligand **4** to AM2 S31N (22-62) with GOLD 5.2 (Jones et al., 1997), using the

Molecular Pharmacology Fast Forward. Published on June 7, 2019 as DOI: 10.1124/mol.119.116640
This article has not been copyedited and formatted. The final version may differ from this version.

GoldScore scoring function (Verdonk et al., 2005). The region of interest used by GOLD was defined to contain the atoms that were within ~15 Å of the compound **1** binding site in the structure. For all the parameters of GOLD 5.2 default values were used, apart from the "allow early termination" that was skipped. Ligand **4** was submitted to 30 genetic algorithm runs. Ten docking poses were produced which were visually inspected using the UCSF Chimera package (Pettersen et al., 2004). The docking pose with the best GoldScore score was used for the subsequent MD simulations. The L46P was manually applied in the simulated AM2 S31N (22-62) to produce AM2 S31N/L46P *apo* protein. MD simulations of AM2 S31N/L46P in hydrated POPC for 1 μs produced a well equilibrated *apo* protein AM2 S31N/L46P structure; its complex with **4** was produced after docking **4** to AM2 S31N/L46P as described above. AM2 WT (22-62) was superimposed with AM2 WT (22-46) – **1** complex (PDB:2KQT) which after deletion of AM2 WT (22-46) afforded the complex of AM2 WT (22-62) with compound **1**. The L46P mutation resulted in the AM2 L46P – **1** complex.

Molecular dynamics (MD) simulations. The proteins AM2 S31N, AM2 S31N/L46P and the complexes AM2 S31N – **4**, AM2 S31N/L46P – **4** and AM2 L46P – **1** were embedded in a hydrated POPC bilayer extending 10x10x20 $Å^3$ in the XYZ directions from the channel. For the membrane insertion, neutralization, the System Builder module of Desmond was used (Schrödinger Release 2018-1: Maestro, Schrödinger, LLC, New York, NY, 2018; Desmond Molecular Dynamics System, Version 3.0, D.E. Shaw Research, New York, NY, 2011.Pdf). Periodic boundary conditions were applied in 75 x 75 x 95 $Å^3$, including 107 POPC lipids. A 20 Å area above and below the protein included 9,636 waters. The total number of atoms included the protein inside the hydrated bilayer was ~ 47,000 atoms. The systems were neutralized by

Molecular Pharmacology Fast Forward. Published on June 7, 2019 as DOI: 10.1124/mol.119.116640
This article has not been copyedited and formatted. The final version may differ from this version.

adding Na^+ ions. A 0.15 M NaCl solution was added. Ligands **1** and **4** were positively charged (+1) using Schrödinger 2017-1 Maestro platform. The H37 residues of AM2 TM were protonated at Nε2 because this form was found to be most populated, and four uncharged H37 residues were applied (Hu et al., 2010; Sharma et al., 2010). The TIP3P (Jorgensen et al., 1983) was applied as the water model and the Schrödinger's viparr utility was used to assign CHARMM36 parameters in protein, lipids and ions (Best et al., 2012).

All simulations were run with the Desmond MD algorithm (Bowers and Shaw, 2006), as implemented by Schrödinger Inc. (Schrödinger Release 2017-1: Desmond Molecular Dynamics System, D. E. Shaw Research, New York, NY, 2017. Maestro-Desmond Interoperability Tools, Schrödinger, New York, NY, 2017). Particle mesh Ewald (PME) was employed to calculate long-range electrostatic interactions (Darden et al., 1993; Essmann et al., 1995) with a grid spacing of 0.8 Å. The Shake method was used to keep all bonds with hydrogen rigid, at ideal lengths and angles (Ryckaert et al., 1977). Van der Waals and short-range electrostatic interactions were smoothly truncated at 9.0 Å. The Nosé-Hoover thermostat was utilized and the Martyna-Tobias-Klein method (Martyna et al., 1994) was used for pressure control. The equations of motion were integrated using the multistep RESPA integrator (Humphreys et al., 1994) with an inner time step of 2.0 fs for bonded interactions and non-bonded interactions within the cutoff. An outer time step of 6.0 fs was used for non-bonded interactions beyond the cut-off. Periodic boundary conditions were applied. For all MD simulations the same relaxation protocol was used. In short, two rounds of steepest descent minimization were performed one with a maximum of 2,000 steps and a harmonic restraint of 50 kcal mol^{-1} $Å^{-2}$ on all heavy solute atoms and a second of 10,000 steps without restraints. Next, a series of MD simulations was performed. The first simulation was performed for 200 ps starting at 10 K with

Molecular Pharmacology Fast Forward. Published on June 7, 2019 as DOI: 10.1124/mol.119.116640
This article has not been copyedited and formatted. The final version may differ from this version.

gradual heating until 310 K in the NVT ensemble with the solute heavy atoms restrained with a force constant of 50 kcal mol^{-1} $Å^{-2}$. The temperature of 308 K was used in our MD simulations in order to ensure that the membrane state is above the melting temperature state of POPC lipids (Koynova and Caffrey, 1998). The heating was followed by equilibration runs. One for 1000 ps simulation in the NPT ensemble with the solute heavy atoms restrained with a force constant of 10 kcal mol^{-1} $Å^{-2}$ to equilibrate solvent and lipids. Next a 10 ns NPT ensemble simulation with 10 kcal mol^{-1} $Å^{-2}$ on solute atoms was run. Two NPT MD simulations, 1000 ps each were followed. In the first harmonic constraints were gradually decreased from 10.0 to 2.0 kcal mol^{-1} $Å^{-2}$ on solute heavy atoms and retaining 2.0 kcal mol^{-1} $Å^{-2}$ constraints on all other solute atoms. Next all harmonic constraints were removed except a 2.0 kcal mol^{-1} $Å^{-2}$ set on protein C_α atoms. This equilibration protocol was followed by a NPT simulation without restraints for 1 μs for the *apo* proteins and 100 ns for the complexes. The replicas of the system were saved every 10 ps. Within this simulation time, the total energy and RMSD of the of the protein backbone Cα atoms (Lyman and Zuckerman, 2006) reached a plateau, and the systems were considered equilibrated and suitable for statistical analysis. For the calculation of protein-lipid hydrogen bonds, a cutoff angle of 20 º between the donor-hydrogen-acceptor atoms and a cutoff distance of 3.2 Å between the donor and acceptor atoms were applied. The snapshots of the different poses were created with Maestro's implementation of PyMol and VMD (Schrödinger Release 2017-1: Maestro, Schrödinger, LLC, New York, NY, 2017) (Humphrey et al., 1996) and UCSF Chimera package (Pettersen et al., 2004). MD simulations were run in workstations and ARIS supercomputer using the GPU implementation and parallel CPU algorithms of MD simulations codes as provided by Desmond (Schrödinger Release 2017-1: Desmond Molecular Dynamics System, D. E. Shaw

Molecular Pharmacology Fast Forward. Published on June 7, 2019 as DOI: 10.1124/mol.119.116640
This article has not been copyedited and formatted. The final version may differ from this version.

Research, New York, NY, 2017; Maestro-Desmond Interoperability Tools, Schrödinger, New York, NY, 2017).

Computation of relative binding free energies by the Molecular Mechanics with Generalized Born and Surface Area continuum solvation (MM-GBSA) approach. Relative binding free energies of aminoadamantane compounds were estimated by the 1-trajectory MM-GBSA (Homeyer and Gohlke, 2012) approach using the relevant module in Schrödinger Suite (Schrödinger Release 2017-1: Maestro, Schrödinger, LLC, New York, NY, 2017). Effective binding energies ($\Delta G_{\text{effective}}$) (Homeyer and Gohlke, 2012; Homeyer et al., 2016) were computed considering the gas phase energy and solvation free energy contributions to binding. $\Delta G_{\text{effective}}$ values were calculated by performing two independent MD simulations for each complex. For this, structural ensembles were extracted in intervals of 20 ps from the last 20 ns of the production simulations of the AM2 – ligand complexes. Prior to the calculations all water molecules, ions, and lipids were removed, and the structures were positioned such that the geometric center of AM2 was located at the coordinate origin. Molecular mechanics energies and the non-polar contribution to the solvation free energy were calculated. The polar part of the solvation free energy was determined by Generalized Born (GB) calculations (Baker et al., 2001; Holst and Saied, 1993; Holst and Saied, 1995). In these calculations, a dielectric constant of $\varepsilon_{\text{solute}} = 1$ was assigned to AM2. Using an implicit solvent representation for the calculation of the effective binding energy is an approximation to reduce the computational costs of the calculations. Previous studies reported on differences in the number of direct interactions of the amino group of different aminoadamantane compounds with waters (Gkeka et al., 2013; Ioannidis et al., 2016). In the present work it is valid to use this approximation because relative water accessibilities of the acceptor groups of the ligand with an orientation of the polar head

Molecular Pharmacology Fast Forward. Published on June 7, 2019 as DOI: 10.1124/mol.119.116640
This article has not been copyedited and formatted. The final version may differ from this version.

towards the N-end or the C-end were similar. Entropy effects were ignored assumed to be similar for the complexes of ligand **4** with the two proteins AM2 S31N and AM2 S31N/L46P and **1** with AM2 WT and AM2 L46P.

RESULTS

Resistance selection against the AM2 S31N inhibitor 4. Hypothesis-driven optimization of the pharmacokinetic properties of isoxazole-conjugated AM2 S31N inhibitors led to the development of compound **4** (Wang et al., 2018). Electrophysiological assays showed that compound **4** blocked the AM2 S31N proton channel with a K_d of 4.5 ± 1.0 μM (Wang et al., 2018). In antiviral plaque assays, compound **4** inhibited multiple oseltamivir-sensitive and -resistant influenza A viruses with submicromolar EC_{50} values. Compound **4** was also well tolerated in MDCK cells having low cytotoxicity (CC_{50} > 300 μM) and had favorable *in vitro* pharmacokinetic properties, showing a half-life greater than 145 min in mouse microsomes and high membrane permeability in Caco-2 cells (Wang et al., 2018). Unlike previously designed AM2 S31N inhibitors, compound **4** was found to have slow K_{on} and K_{off} values in kinetic studies. In order to profile the drug resistance mechanism of this newly developed inhibitor, the 2009 H1N1 pandemic virus A/California/07/2009 (H1N1) was passaged under increasing drug selection pressure of compound **4**. This virus is among the circulating influenza strains resistant to amantadine. In the passage experiment, the initial drug concentration was set as 1×EC_{50} concentration as determined using plaque reduction assays. For passage 0 virus (P0), no plaques were observed at 30 μM of compound **4**. At passage 04 (P4), the drug selection pressure was set at 8×EC_{50}. When compound **4** was tested against P4 viruses, several plaques were observed in the presence of 30 μM of **4**, compared with no plaques for the P0, P2, or P3 viruses (**Fig. 3A** &

Molecular Pharmacology Fast Forward. Published on June 7, 2019 as DOI: 10.1124/mol.119.116640
This article has not been copyedited and formatted. The final version may differ from this version.

B) (**Table 1**), indicating the emergence of resistance. Although resistant viruses appeared at P4, there was still a noticeable reduction in the overall number of plaques compared with the virus only. Therefore, the calculated EC_{50} remained unchanged (**Fig. 3B**) (**Table 1**). At passage 05 (P5), the drug selection pressure was increased to $16\times EC_{50}$. The P5 virus showed drastic resistance, as a significant amount of plaques remained in the presence of 30 μM of compound **4** (**Fig. 3**).

To determine the resistance mutation, the P5 viral gene segment that encodes for the AM2 channel was sequenced. Compared to the P0 virus which only had the S31N mutation, the P5 virus had an additional mutation, L46P, located at the end of the AM2 transmembrane helices. In order to rule out the possibility that other mutations existed in the viral genome that might influence drug sensitivity, whole-genome sequencing was performed for the P5 virus. Only the L46P mutation in the AM2 segment was found in P5 viruses when compared to the whole-genome sequence of the P0 viruses. The AM2 S31N/L46P was found in less than 0.01% of clinically isolated human influenza A viruses in the Influenza Research Database (http://www.fludb.org) (data not shown), suggesting that L46P is a rare mutant among circulating viruses. Nevertheless, the presence of L46P in the database means that this mutant may exist naturally independent of drug selection pressure. Interestingly, the L46P mutation was no longer observed in the sequenced AM2 gene when the P5 resistant viruses underwent three additional passages in the absence of compound **4** (**Table 1**). Therefore, this mutation might not be favored in the absence of drug pressure.

Electrophysiological assay confirmed drug resistance of AM2 S31N/L46P against compound 4. Electrophysiological two-electrode voltage clamp (TEVC) measurements have been previously utilized as a reliable and robust tool to evaluate the function and inhibition of

Molecular Pharmacology Fast Forward. Published on June 7, 2019 as DOI: 10.1124/mol.119.116640
This article has not been copyedited and formatted. The final version may differ from this version.

AM2 as well as the pharmacological properties of AM2 channel blockers. As expected, 100 μM amantadine (**1**) displayed marginal inhibition against the AM2 S31N (Wang et al., 2013b), whereas AM2 S31N inhibitors (compounds **2**-**6**) showed 47.9-90.6% inhibition at the 2-minute time point after application (Li et al., 2017; Wang et al., 2018) (**Fig. 4A**, left column).

In order to investigate the AM2 S31N/L46P channel conductance and inhibition, the mutation was introduced in the pGEM3 vector. In agreement with the drug resistance selection, compounds **2**-**6** showed almost no inhibition on the proton conductance of AM2 S31N/L46P channels (**Fig. 4A**, right column). Specific conductance measurements were carried out to determine the effects on function due to the introduction of the L46P mutation. The current was plotted against the immunosignal in order to obtain a slope that correlates with the specific conductance. Overall, no significant change in proton conductance profile was observed between AM2 S31N channels and the mutated AM2 S31N/L46P (**Fig. 4B**), suggesting AM2 S31N/L46P remains a proton-selective channel.

To determine whether L46P affects the drug sensitivity of amantadine (**1**), the AM2 L46P mutant was constructed. As previously reported, amantadine (**1**) significantly inhibits WT channels, having 92.9% inhibition against 100 μM compound concentration at the 2-minute time point (**Fig. 4C)**. Interestingly, it was found that the L46P in WT channels did not significantly change amantadine sensitivity with 91% inhibition. Compound **4** was unable to inhibit AM2 L46P channels, as shown in the comparison of conductance plots for **1** against AM2 WT and AM2 L46P with **4** against AM2 L46P (**Fig. 4C**). These results suggest that L46P disproportionally affect the drug sensitivity of AM2 S31N inhibitors **2**–**6** against AM2 S31N channel, but not the drug sensitivity of amantadine against AM2 WT.

Molecular Pharmacology Fast Forward. Published on June 7, 2019 as DOI: 10.1124/mol.119.116640
This article has not been copyedited and formatted. The final version may differ from this version.

MD simulations of the effect of L46P mutant on drug binding. MD simulations were applied for the *apo* AM2 WT, AM2 S31N and the corresponding mutated *apo* proteins AM2 L46P and AM2 S31N/L46P for 1 μs in order to investigate the conformational properties of these proteins. The MD simulations showed that the L46P induced a γ-turn in local structure. The peptide bond dihedral connecting R45 and L46 which was -172º in AM2 WT and AM2 S31N changed to +1.6º for AM2 L46P and AM2 S31N/L46P. Thus, the L46P mutation produced an important conformational change at the C-end for each AM2 monomer. However, this change occurs simultaneously to all monomers rendering the relative orientation between successive AM2 monomers the same as in the L46 case. The L46P mutation also affected more distant conformational changes in the AM2 TM part of the channel, with the most important for drug action being a broadening of the N-terminus. This conformational change was observed after 350-400 ns in the 1 μs MD simulation of the *apo* protein AM2 S31N/L46P. The 1 μs equilibrated AM2 S31N and AM2 S31N/L46P proteins were then simulated for another 100 ns in complex with compound **4**. In both protein-drug complexes, the system reached equilibration after ~ 70 ns (**Fig. S1**).

In complexes of compound **4** with AM2 S31N or AM2 S31N/L46P proteins, the polar head of the ligand was oriented towards the N-terminus according to the experimental findings (Hu et al., 2018; Wang et al., 2013a; Wu et al., 2014). Ligand was stabilized with similar hydrophilic interactions in both complexes, but different hydrophobic interactions. For the AM2 S31N – **4** complex, the adamantane ring fitted close to Gly34 and the ligand formed hydrogen bond interactions between (a) its NH_2^+ group and isoxazole nitrogen and N31 amino side chains throughout the trajectory and (b) its hydroxyl group and occasionally the backbone Ala30 carbonyls (**Fig. 5A & B**). The same hydrophilic interactions also stabilized compound **4** inside

Molecular Pharmacology Fast Forward. Published on June 7, 2019 as DOI: 10.1124/mol.119.116640
This article has not been copyedited and formatted. The final version may differ from this version.

AM2 S31N/L46P pore (**Fig. 5C**). However, there was a notable difference as regards to the hydrophobic interactions. In the AM2 S31N – **4** complex, the isoxazole-cyclopropyl fragment of compound **4** forms hydrophobic interactions with V27 side chain isopropyl groups. This hydrophobic interaction was lost in the AM2 S31N/L46P mutant due to the channel broadening at the N-terminus between residues 22-31. Superposition between AM2 S31N and AM2 S31N/L46P complexes with compound **4** clearly revealed this conformational change that L46P mutation effected (**Fig. 5D**). The AM2 S31N/L46P mutant pore seems to broaden significantly between residues 22-31, compared to the AM2 S31N counterpart, making compound **4** unable to prevent the water molecules from entering the pore (**Fig. 5C**).

MM-GBSA binding free energy calculations from two independent MD simulations resulted in a more negative $\Delta G_{effective}$ for AM2 S31N – **4** complex by more than 22.2 kcal mol^{-1} compared to AM2 S31N/L46P – **4** complex (**Table 2**) suggesting a considerably more stable complex for **4** to AM2 S31N.

Next, MD simulations were applied for AM2 WT and AM2 L46P in complex with amantadine **(Fig. 6)**. While AM2 S31N and AM2 S31N/L46P mutant showed differential drug sensitivity towards compound **4**, amantadine readily blocked both the AM2 WT and AM2 L46P mutant according to the MD simulations (**Fig. 6A & B**). This observation was consistent with the electrophysiological results in which amantadine showed potent channel inhibition against AM2 WT and AM2 L46P (**Fig. 4C**). Interestingly, although L46P similarly broadened the channel pore at the N-terminus in the AM2 L46P mutant, it only affects residues between 22-31 and not between residues 31-34 where amantadine binds. Indeed, in the MD simulations of AM2 L46P with amantadine, no water was observed to pass through the channel (**Fig. 6B**). Consequently, superposition between AM2 WT and AM2 L46P complexes showed similar interactions

Molecular Pharmacology Fast Forward. Published on June 7, 2019 as DOI: 10.1124/mol.119.116640
This article has not been copyedited and formatted. The final version may differ from this version.

stabilizing amantadine (**Fig. 6C**). MM-GBSA calculations from two independent MD simulations resulted in $\Delta G_{effective}$ values, for **1** bound to AM2 WT and AM2 L46P differing by less than 4 kcal mol^{-1}. This difference in binding energy value corresponds to the accuracy of the calculations method and suggest that the binding affinities are similar (**Table 2**).

DISCUSSION

The conjugates of amantadine and polar head heterocycles represent useful leads of a new generation of anti-influenza A drugs. In this study, serial viral passaging experiments were performed to select escape variants that are resistant to one of our advanced lead compound, **4**. Unlike previously identified drug-resistant AM2 mutants which had mutations along the N-terminus of the channel between residues 26-34, a novel drug-resistant mutation L46P located at the C-end of the AM2 transmembrane helices and is distal from the drug binding site of the N-terminus of the channel pore was identified. Drug resistance of AM2 S31N/L46P mutant against compound **4** was confirmed in both electrophysiological assay and the antiviral plaque assay. Interestingly, AM2 L46P remained sensitive to amantadine. To elucidate the differential effect of L46P on the drug sensitivity of AM2 S31N inhibitor **4** and AM2 WT inhibitor amantadine, MD simulations and MM-GBSA calculations were performed on these protein ligand complexes. The mutation found at L46P broadened the drug-binding site at the N-terminus of the channel, specifically between residues 22-31, in both the AM2 L46P and AM2 S31N/L46P mutants. However, this only affects the binding of AM2 S31N inhibitors such as compound **4** as it abolished the critical hydrophobic interaction between the lipophilic heterocyclic part of the drug and V27 side chains. In contrast, the L46P mutation had minimal effect on amantadine binding as this compound binds between residues 31-34, which was not altered in pore diameter due to L46P mutation. In other words, the L46P affected the region beyond the amantadine-binding site.

Molecular Pharmacology Fast Forward. Published on June 7, 2019 as DOI: 10.1124/mol.119.116640
This article has not been copyedited and formatted. The final version may differ from this version.

Overall, MD simulations and MM-GBSA calculations provided an explanation for this allosteric resistance mechanism. To our knowledge, L46P is the first drug-resistant AM2 mutant located below H37 that was experimentally confirmed.

It should be noted that Santer et al. has recently reported only marginal inhibition of AM2 L46P by amantadine in a proton flux (pHlux) assay in AM2-expressing *Escherichia coli* (Santner et al., 2018a; Santner et al., 2018b). In their study, AM2 with random mutations was expressed in *E. coli*, and the proton flux and drug sensitivity were quantified using the pH sensitive green fluorescent protein, pHluorin. In their results, it was shown that a single L46P mutant was resistant to amantadine and a few other analogs. Intriguingly, the M2 variant M_060 which contained two extra V7L/G16C mutants in the N-terminus besides L46P displayed amantadine sensitivity similar to what we observed in our L46P alone using A/California/07/09 background. It appears that amantadine showed sequence-dependent drug sensitivities for N31S/L46P variants in their bacteria flux assay. It was also noted that two potent AM2 V27A channel blockers developed by us, Spm and Spa (Balannik et al., 2009), had minimal channel inhibition when tested in their bacteria flux assay against the AM2 V27A single mutant. Taken together, the bacteria flux assay results appear to be not consistent with the TEVC and antiviral assay results, which raises a concern whether the bacteria flux assay can be applied to accurately characterize channel blockage and predict the antiviral efficacy of M2 channel blockers. We cannot provide an accurate explanation for this discrepancy since we do not know the exact experimental details of the bacteria flux assay. One reason might be that the differences in the lipid composition between *E. coli* and *Xenopus* oocyte membranes contribute to the method-specific variations in the activity and inhibition profiles (Zhou and Cross, 2013). Moreover, the transporters and channels expressed in *E. coli* might compromise the assay results. Nevertheless,

Molecular Pharmacology Fast Forward. Published on June 7, 2019 as DOI: 10.1124/mol.119.116640
This article has not been copyedited and formatted. The final version may differ from this version.

our electrophysiological assay results showed that AM2 L46P mutant remained sensitive to amantadine, and this result was also supported by the MD simulation and MM-GBSA calculations.

The design of successful antiviral therapeutics requires consideration and evaluation for the likelihood of resistance, since a substandard barrier to resistance can derail the development of an otherwise efficacious drug candidate. The drivers of drug resistance depend on the inhibitor as well as the protein target. For AM2, the amino acid changes allowed that still preserves the functionality of the protein necessary for viral replication appears to be limited, as studied by Balannik et al (Balannik et al., 2010). It likely correlates that drug resistance for new AM2 inhibitors are limited to a subset of mutant variants. Up until now, drug resistance selection in viral passage experiments have identified amino acid changes at or near the drug binding site. The newly identified L46P AM2 in replicating viruses represents a new resistance strategy that influenza can adopt when under drug selection pressure. In regard to AM2 antiviral development, the next generation of AM2-S31N inhibitor might need to focus on the region between S31 and H37 in order to avoid the allosteric effect of L46P mutant. Moreover, the disappearance of L46P mutation after drug withdrawal as well as its low abundance in circulating strain populations suggest that strains containing this AM2 variant may have limited persistence. The reason for this remains unclear, as we did not observe any changes in the proton conductance activity of L46P AM2 channels. Moreover, additional research is needed to evaluate whether compensatory mutations can arise that may increase persistence. An important point to be considered in future drug discovery campaigns is how subtle changes in the overall structure of the AM2 can have dramatic effects on the efficacy for developing drugs. Because the lipid composition can influence membrane protein structure, the advent of improved structural biology

Molecular Pharmacology Fast Forward. Published on June 7, 2019 as DOI: 10.1124/mol.119.116640
This article has not been copyedited and formatted. The final version may differ from this version.

techniques that can resolve native-like conformations will greatly aid in the design of future channel blockers.

Acknowledgments

This work was supported by computational time granted from the Greek Research & Technology Network (GRNET) in the National HPC facility – ARIS – under project IDs pr005010).

Author Contributions

Participated in research design: Rami Musharrafieh, Chunlong Ma, Antonios Kolocouris, and Jun Wang.

Conducted experiments: Rami Musharrafieh, Panagiotis I. Lagarias, Chunlong Ma, and Gene Tan.

Contributed new reagents or analytic tools: Rami Musharrafieh, Panagiotis I. Lagarias, Chunlong Ma, Gene Tan, Antonios Kolocouris, and Jun Wang.

Performed data analysis: Rami Musharrafieh, Panagiotis I. Lagarias, Chunlong Ma, Gene Tan, Antonios Kolocouris, and Jun Wang.

Wrote or contributed to the writing of the manuscript: Rami Musharrafieh, Antonios Kolocouris, and Jun Wang.

References

Acharya R, Carnevale V, Fiorin G, Levine BG, Polishchuk AL, Balannik V, Samish I, Lamb RA, Pinto LH, DeGrado WF and Klein ML (2010) Structure and Mechanism of Proton Transport Through the Transmembrane Tetrameric M2 Protein Bundle of the Influenza A Virus. *Proc Natl Acad Sci USA* **107**(34): 15075-15080.

Molecular Pharmacology Fast Forward. Published on June 7, 2019 as DOI: 10.1124/mol.119.116640
This article has not been copyedited and formatted. The final version may differ from this version.

Baker NA, Sept D, Joseph S, Holst MJ and McCammon JA (2001) Electrostatics of Nanosystems: Application to Microtubules and the Ribosome. *Proc Natl Acad Sci USA* **98**(18): 10037-10041.

Balannik V, Carnevale V, Fiorin G, Levine BG, Lamb RA, Klein ML, DeGrado WF and Pinto LH (2010) Functional Studies and Modeling of Pore-Lining Residue Mutants of the Influenza A Virus M2 Ion Channel. *Biochemistry* **49**(4): 696-708.

Balannik V, Wang J, Ohigashi Y, Jing X, Magavern E, Lamb RA, DeGrado WF and Pinto LH (2009) Design and Pharmacological Characterization of Inhibitors of Amantadine-Resistant Mutants of the M2 Ion Channel of Influenza A Virus. *Biochemistry* **48**(50): 11872-11882.

Best RB, Zhu X, Shim J, Lopes PEM, Mittal J, Feig M and MacKerell AD (2012) Optimization of the Additive CHARMM All-Atom Protein Force Field Targeting Improved Sampling of the Backbone phi, psi and Side-Chain chi(1) and chi(2) Dihedral Angles. *J Chem Theory Comput* **8**(9): 3257-3273.

Bowers KJS, F. D. Salmon, J. K. Shan, Y. and Shaw DEC, E. Xu, H. Dror, R. O. Eastwood, M. P. Gregersen, B. A. Klepeis, J. L. Kolossvary, I. Moraes, M. A. (2006) Molecular Dynamics---Scalable Algorithms for Molecular Dynamics Simulations on Commodity Clusters. , in *Proceedings of the 2006 ACM/IEEE conference on Supercomputing* p 84, ACM Press: New York, New York, USA, SC.

Cady SD and Hong M (2008) Amantadine-Induced Conformational and Dynamical Changes of the Influenza M2 Transmembrane Proton Channel. *Proc Natl Acad Sci USA* **105**(5): 1483-1488.

Molecular Pharmacology Fast Forward. Published on June 7, 2019 as DOI: 10.1124/mol.119.116640
This article has not been copyedited and formatted. The final version may differ from this version.

Cady SD, Schmidt-Rohr K, Wang J, Soto CS, Degrado WF and Hong M (2010) Structure of the amantadine binding site of influenza M2 proton channels in lipid bilayers. *Nature* **463**(7281): 689-692.

Chen BJ, Leser GP, Jackson D and Lamb RA (2008) The Influenza Virus M2 Protein Cytoplasmic Tail Interacts with the M1 Protein and Influences Virus Assembly at the Site of Virus Budding. *J Virol* **82**(20): 10059-10070.

Darden T, York D and Pedersen L (1993) Particle Mesh Ewald: An Nlog(N) Method for Ewald Sums in Large Systems. *J Chem Phys* **98**(12): 10089-10092.

Essmann U, Perera L, Berkowitz ML, Darden T, Lee H and Pedersen LG (1995) A Smooth Particle Mesh Ewald Method. *J Chem Phys* **103**(19): 8577-8593.

Gkeka P, Eleftheratos S, Kolocouris A and Cournia Z (2013) Free Energy Calculations Reveal the Origin of Binding Preference for Aminoadamantane Blockers of Influenza A/M2TM Pore. *J Chem Theory Comput* **9**(2): 1272-1281.

Halgren TA (1996) Merck Molecular Force Field. 1. Basis, Form, Scope, Parameterization, and Performance of MMFF94. *J Comput Chem* **17**(5-6): 490-519.

Holst M and Saied F (1993) Multigrid Solution of the Poisson - Boltzmann Equation. *J Comput Chem* **14**(1): 105-113.

Holst MJ and Saied F (1995) Numerical Solution of the Nonlinear Poisson–Boltzmann Equation: Developing More Robust and Efficient Methods. *J Comput Chem* **16**(3): 337-364.

Homeyer N and Gohlke H (2012) Free Energy Calculations by the Molecular Mechanics Poisson-Boltzmann Surface Area Method. *Mol Inform* **31**(2): 114-122.

Homeyer N, Ioannidis H, Kolarov F, Gauglitz G, Zikos C, Kolocouris A and Gohlke H (2016) Interpreting Thermodynamic Profiles of Aminoadamantane Compounds Inhibiting the

Molecular Pharmacology Fast Forward. Published on June 7, 2019 as DOI: 10.1124/mol.119.116640
This article has not been copyedited and formatted. The final version may differ from this version.

M2 Proton Channel of Influenza A by Free Energy Calculations. *J Chem Inf Model* **56**(1): 110-126.

Hu FH, Luo WB and Hong M (2010) Mechanisms of Proton Conduction and Gating in Influenza M2 Proton Channels from Solid-State NMR. *Science* **330**(6003): 505-508.

Hu YM, Hau RK, Wang YX, Tuohy P, Zhang YT, Xu ST, Ma CL and Wang J (2018) Structure-Property Relationship Studies of Influenza A Virus AM2-S31N Proton Channel Blockers. *ACS Med Chem Lett* **9**(11): 1111-1116.

Humphrey W, Dalke A and Schulten K (1996) VMD: Visual Molecular Dynamics. *J Mol Graph Model* **14**(1): 33-38.

Humphreys DD, Friesner RA and Berne BJ (1994) A Multiple-Time-Step Molecular Dynamics Algorithm for Macromolecules. *J Phys Chem* **98**(27): 6885-6892.

Ioannidis H, Drakopoulos A, Tzitzoglaki C, Homeyer N, Kolarov F, Gkeka P, Freudenberger K, Liolios C, Gauglitz G, Gohlke H and Kolocouris A (2016) Alchemical Free Energy Calculations and Isothermal Titration Calorimetry Measurements of Aminoadamantanes Bound to the Closed State of Influenza A/M2TM. *J Chem Inf Model* **56**(5): 862-876.

Jing XH, Ma CL, Ohigashi Y, Oliveira FA, Jardetzky TS, Pinto LH and Lamb RA (2008) Functional Studies Indicate Amantadine Binds to the Pore of the Influenza A Virus M2 Proton-Selective Ion Channel. *Proc Natl Acad Sci USA* **105**(31): 10967-10972.

Jones G, Willett P, Glen RC, Leach AR and Taylor R (1997) Development and Validation of a Genetic Algorithm for Flexible Docking. *J Mol Biol* **267**(3): 727-748.

Jorgensen WL, Chandrasekhar J, Madura JD, Impey RW and Klein ML (1983) Comparison of Simple Potential Functions for Simulating Liquid Water. *J Chem Phys* **79**(2): 926-935.

Molecular Pharmacology Fast Forward. Published on June 7, 2019 as DOI: 10.1124/mol.119.116640
This article has not been copyedited and formatted. The final version may differ from this version.

Koynova R and Caffrey M (1998) Phases and Phase Transitions of the Phosphatidylcholines. *Biochim Biophys Acta Biomembr* **1376**(1): 91-145.

Kwon B and Hong M (2016) The Influenza M2 Ectodomain Regulates the Conformational Equilibria of the Transmembrane Proton Channel: Insights from Solid-State Nuclear Magnetic Resonance. *Biochemistry* **55**(38): 5387-5397.

Li F, Hu YM, Wang YX, Ma CL and Wang J (2017) Expeditious Lead Optimization of Isoxazole-Containing Influenza A Virus M2-S31N Inhibitors Using the Suzuki-Miyaura Cross-Coupling Reaction. *J Med Chem* **60**(4): 1580-1590.

Lyman E and Zuckerman DM (2006) Ensemble-Based Convergence Analysis of Biomolecular Trajectories. *Biophysical J* **91**(1): 164-172.

Ma CL, Fiorin G, Carnevale V, Wang J, Lamb RA, Klein ML, Wu YB, Pinto LH and DeGrado WF (2013) Asp44 Stabilizes the Trp41 Gate of the M2 Proton Channel of Influenza A Virus. *Structure* **21**(11): 2033-2041.

Ma CL, Polishchuk AL, Ohigashi Y, Stouffer AL, Schon A, Magavern E, Jing XH, Lear JD, Freire E, Lamb RA, DeGrado WF and Pinto LH (2009) Identification of the Functional Core of the Influenza A Virus A/M2 Proton-Selective Ion Channel. *Proc Natl Acad Sci USA* **106**(30): 12283-12288.

Ma CL and Wang J (2018) Functional Studies Reveal the Similarities and Differences Between AM2 and BM2 Proton Channels from Influenza Viruses. *Biochim Biphys Acta Biomembr* **1860**(2): 272-280.

Ma CL, Zhang JT and Wang J (2016) Pharmacological Characterization of the Spectrum of Antiviral Activity and Genetic Barrier to Drug Resistance of M2-S31N Channel Blockers. *Mol Pharmacol* **90**(3): 188-198.

Molecular Pharmacology Fast Forward. Published on June 7, 2019 as DOI: 10.1124/mol.119.116640
This article has not been copyedited and formatted. The final version may differ from this version.

Martyna GJ, Tobias DJ and Klein ML (1994) Constant Pressure Molecular Dynamics Algorithms. *J Chem Phys* **101**(5): 4177-4189.

McCown MF and Pekosz A (2006) Distinct Domains of the Influenza A Virus M2 Protein Cytoplasmic Tail Mediate Binding to the M1 Protein and Facilitate Infectious Virus Production. *J Virol* **80**(16): 8178-8189.

Musharrafieh R, Ma CL and Wang J (2018) Profiling the in vitro drug-resistance mechanism of influenza A viruses towards the AM2-S31N proton channel blockers. *Antiviral Res* **153**: 10-22.

Park EK, Castrucci MR, Portner A and Kawaoka Y (1998) The M2 Ectodomain is Important for its Incorporation into Influenza A Virions. *J Virol* **72**(3): 2449-2455.

Pettersen EF, Goddard TD, Huang CC, Couch GS, Greenblatt DM, Meng EC and Ferrin TE (2004) UCSF Chimera - A Visualization System for Exploratory Research and Analysis. *J Comput Chem* **25**(13): 1605-1612.

Pinto LH, Holsinger LJ and Lamb RA (1992) Influenza virus M2 protein has ion channel activity. *Cell* **69**: 517-528.

Rossman JS, Jing XH, Leser GP and Lamb RA (2010) Influenza Virus M2 Protein Mediates ESCRT-Independent Membrane Scission. *Cell* **142**(6): 902-913.

Ryckaert JP, Ciccotti G and Berendsen HJC (1977) Numerical Integration of the Cartesian Equations of Motion of a System with Constraints: Molecular Dynamics of N-Alkanes. *J Comput Phys* **23**(3): 327-341.

Santner P, Martins J, Kampmeyer C, Hartmann-Petersen R, Laursen JS, Stein A, Olsen CA, Arkin IT, Winther JR, Willemoes M and Lindorff-Larsen K (2018a) Random

Molecular Pharmacology Fast Forward. Published on June 7, 2019 as DOI: 10.1124/mol.119.116640
This article has not been copyedited and formatted. The final version may differ from this version.

Mutagenesis Analysis of the Influenza A M2 Proton Channel Reveals Novel Resistance Mutants. *Biochemistry* **57**(41): 5957-5968.

Santner P, Martins JMD, Laursen JS, Behrendt L, Riber L, Olsen CA, Arkin IT, Winther JR, Willemoes M and Lindorff-Larsen K (2018b) A Robust Proton Flux (pHlux) Assay for Studying the Function and Inhibition of the Influenza A M2 Proton Channel. *Biochemistry* **57**(41): 5949-5956.

Schmidt NW, Mishra A, Wang J, DeGrado WF and Wong GCL (2013) Influenza Virus A M2 Protein Generates Negative Gaussian Membrane Curvature Necessary for Budding and Scission. *J Am Chem Soc* **135**(37): 13710-13719.

Sharma M, Yi MG, Dong H, Qin HJ, Peterson E, Busath DD, Zhou HX and Cross TA (2010) Insight into the Mechanism of the Influenza A Proton Channel from a Structure in a Lipid Bilayer. *Science* **330**(6003): 509-512.

Stouffer AL, Acharya R, Salom D, Levine AS, Di Costanzo L, Soto CS, Tereshko V, Nanda V, Stayrook S and DeGrado WF (2008) Structural Basis for the Function and Inhibition of an Influenza Virus Proton Channel. *Nature* **452**(7185): 380-380.

Takeda M, Pekosz A, Shuck K, Pinto LH and Lamb RA (2002) Influenza A virus M-2 ion channel activity is essential for efficient replication in tissue culture. *J Virol* **76**(3): 1391-1399.

Tang YJ, Zaitseva F, Lamb RA and Pinto LH (2002) The Gate of the Influenza Virus M-2 Proton Channel is Formed by a Single Tryptophan Residue. *J Biol Chem* **277**(42): 39880-39886.

Molecular Pharmacology Fast Forward. Published on June 7, 2019 as DOI: 10.1124/mol.119.116640
This article has not been copyedited and formatted. The final version may differ from this version.

Thomaston JL, Polizzi NF, Konstantinidi A, Wang J, Kolocouris A and DeGrado WF (2018) Inhibitors of the M2 Proton Channel Engage and Disrupt Transmembrane Networks of Hydrogen-Bonded Waters. *J Am Chem Soc* **140**(45): 15219-15226.

Verdonk ML, Chessari G, Cole JC, Hartshorn MJ, Murray CW, Nissink JWM, Taylor RD and Taylor R (2005) Modeling Water Molecules in Protein-Ligand Docking Using GOLD. *J Med Chem* **48**(20): 6504-6515.

Wang J (2016) M2 as a target to combat influenza drug resistance: what does the evidence say? *Future Virol* **11**(1): 1-4.

Wang J, Li F and Ma C (2015) Recent progress in designing inhibitors that target the drug-resistant M2 proton channels from the influenza A viruses. *Biopolymers* **104**(4): 291-309.

Wang J, Wu YB, Ma CL, Fiorin G, Wang JZ, Pinto LH, Lamb RA, Klein ML and DeGrado WF (2013a) Structure and Inhibition of the Drug-Resistant S31N Mutant of the M2 Ion Channel of Influenza A Virus. *Proc Natl Acad Sci USA* **110**(4): 1315-1320.

Wang JZ, Ma CL, Wang J, Jo H, Canturk B, Fiorin G, Pinto LH, Lamb RA, Klein ML and DeGrado WF (2013b) Discovery of Novel Dual Inhibitors of the Wild-Type and the Most Prevalent Drug-Resistant Mutant, S31N, of the M2 Proton Channel from Influenza A Virus. *J Med Chem* **56**(7): 2804-2812.

Wang YX, Hu YM, Xu ST, Zhang YT, Musharrafieh R, Hau RK, Ma CL and Wang J (2018) In Vitro Pharmacokinetic Optimizations of AM2-S31N Channel Blockers Led to the Discovery of Slow-Binding Inhibitors with Potent Antiviral Activity against Drug-Resistant Influenza A Viruses. *J Med Chem* **61**(3): 1074-1085.

Wu YB, Canturk B, Jo H, Ma CL, Gianti E, Klein ML, Pinto LH, Lamb RA, Fiorin G, Wang J and DeGrado WF (2014) Flipping in the Pore: Discovery of Dual Inhibitors That Bind in

Molecular Pharmacology Fast Forward. Published on June 7, 2019 as DOI: 10.1124/mol.119.116640
This article has not been copyedited and formatted. The final version may differ from this version.

Different Orientations to the Wild-Type versus the Amantadine-Resistant 531N Mutant of the Influenza A Virus M2 Proton Channel. *J Am Chem Soc* **136**(52): 17987-17995.

Zhou HX and Cross TA (2013) Modeling the membrane environment has implications for membrane protein structure and function: Influenza A M2 protein. *Protein Sci* **22**(4): 381-394.

Molecular Pharmacology Fast Forward. Published on June 7, 2019 as DOI: 10.1124/mol.119.116640
This article has not been copyedited and formatted. The final version may differ from this version.

FOOTNOTES

This research was supported by the NIH grants AI119187 and AI144887 to J.W. We thank Chiesi Hellas which supported this research (SARG No 10354) and the State Scholarships Foundation (IKY) for providing a Ph.D fellowship to P.L. (MIS 5000432, NSRF 2014-2020). This project was partly funded with federal funds from the National Institute of Allergy and Infectious Diseases, NIH, Department of Health and Human Services under Award Number U19AI110819.

Molecular Pharmacology Fast Forward. Published on June 7, 2019 as DOI: 10.1124/mol.119.116640
This article has not been copyedited and formatted. The final version may differ from this version.

Figure Legends

Figure 1. AM2 WT inhibitor Amantadine (1) and the AM2 S31N inhibitors 2-6.

Figure 2. AM2 inhibitors are a class of influenza antivirals that bind to the pore of the channel. (A) Influenza AM2 WT (PDB: 6BKK) structure bound with amantadine (1) with the amino group oriented towards the C-terminus and (B) influenza AM2 S31N structure (PDB: 2LY0) in complex with compound (2) with the conjugated isoxazole group positioned at the N-terminus.

Figure 3. Drug resistance for compound 4 selected in cell culture. (A) Viruses from each passage were tested against compound 4 at 30 μM using plaque reduction assay to determine drug susceptibility. The M2 gene was sequenced from passage 00 (original virus stock) and passage 05 (virus that appears resistant to compound 4) in order to map the mutations that give rise to resistance. CTT represents the nucleotide sequence for the lysine residue at position 46, and CCT represents the nucleotide sequence for the proline mutant identified in passage 05. (B) EC_{50} was determined for passage 02-05. At passage 05, the EC_{50} was observed to be > 30 μM. All antiviral EC_{50} values are the mean ± standard deviation of two independent experiments.

Figure 4. TEVC recordings confirm the functional resistance of AM2 S31N/L46P towards S31N inhibitors. (A) Cell culture EC_{50} values against AM2 S31N-containing influenza viruses for compound **1** (Wang et al., 2013b), 2-5 (Wang et al., 2018) and compound **6** (Li et al., 2017) are shown. Ion channel conductance of the AM2 S31N (left column traces) and AM2 S31N/L46P (right column traces) was measured in the presence of 100 μM for compounds 1-6. (B) Specific activities were obtained by plotting the whole-cell current for single intact oocytes against the concentration of AM2 protein detected by immunofluorescence on the oocyte surface. (C) TEVC measurements for AM2 WT and AM2 L46P channels against compound 1 and AM2 L46P channel against compound 4.

Molecular Pharmacology Fast Forward. Published on June 7, 2019 as DOI: 10.1124/mol.119.116640
This article has not been copyedited and formatted. The final version may differ from this version.

Figure 5. MD simulation structures for compound 4 bound to AM2 S31N and AM2 S31N/L46P channels. (A) 2D diagram of the most important interactions between compound 4 and the AM2 S31N (22-62) from the 100 ns MD simulations trajectory. (B) In AM2 S31N (22-62) in complex with compound 4 no water passage was observed between the ligand and N-end which is consistent with protons blockage. (C) In AM2 S31N/L46P (22-62) in complex with compound 4. The L46P mutation produced an N-end broadening that weakened key hydrophobic interactions between V27 residues and the isoxazole-cyclopropyl group of compound 4. (D) Superposition of AM2 S31N (grey) and AM2 S31N/L46P (blue) structures with 4 bound.

Figure 6. MD simulation structures for amantadine (1) bound to AM2 WT and AM2 L46P channels. (A) AM2 WT and (B) AM2 L46P in complex with amantadine (**1)** located near residues 31-34 within the pore. Amantadine prevented entrance of waters from the N-end of the AM2 L46P. (C) Superposition of AM2 WT (grey) and AM2 L46P (blue) with amantadine (**1**) bound. The AM2 L46P is wider from the AM2 WT in the N-end but are equally wide to the C-end enabling amantadine to block protons passage.

Molecular Pharmacology Fast Forward. Published on June 7, 2019 as DOI: 10.1124/mol.119.116640
This article has not been copyedited and formatted. The final version may differ from this version.

Tables

Table 1. Drug Resistance Selection

Passage Number[a]	Compound **4** Selection Pressure (μM)	EC_{50} (μM)[b]	Mutation[c]
0	N/A	0.8 ± 0.05	WT
1	0.75	N.D.	N.D.
2	1.5	1.5 ± 0.4	N.D.
3	3	1.1 ± 0.3	N.D.
4	6	0.7 ± 0.4	N.D.
5	12	>30 (Resistant)	L46P
6	24	N.D.	L46P
7	0	N.D.	N.D.
8	0	N.D.	L46 + P46
9	0	N.D.	P46L

[a]Influenza Virus A/California/07/2009 (H1N1) was passaged at an MOI of 0.001 in MDCK cells.

[b]EC_{50} values were determined by plaque assay (mean ± standard deviation of two independent experiments).

[c]The M segment encoding for the AM2 protein was sequenced.

Molecular Pharmacology Fast Forward. Published on June 7, 2019 as DOI: 10.1124/mol.119.116640
This article has not been copyedited and formatted. The final version may differ from this version.

Table 2. MM-GBSA calculated free energy of binding

Compound	AM2 channel[a]	$\Delta G_{effective}$ (kcal·mol^{-1})[b]
1	WT	-36.3 ± 2.5
	L46P	-40.2 ± 2.5
4	S31N	-64.1 ± 2.5
	S31N/L46P	-41.9 ± 2.1

[a]AM2 – ligand structures were simulated as described in the main text.

[b]Binding free energies ± standard deviation from two independent MD simulations for each complex.

Molecular Pharmacology Fast Forward. Published on June 7, 2019 as DOI: 10.1124/mol.119.116640
This article has not been copyedited and formatted. The final version may differ from this version.

Figure 1

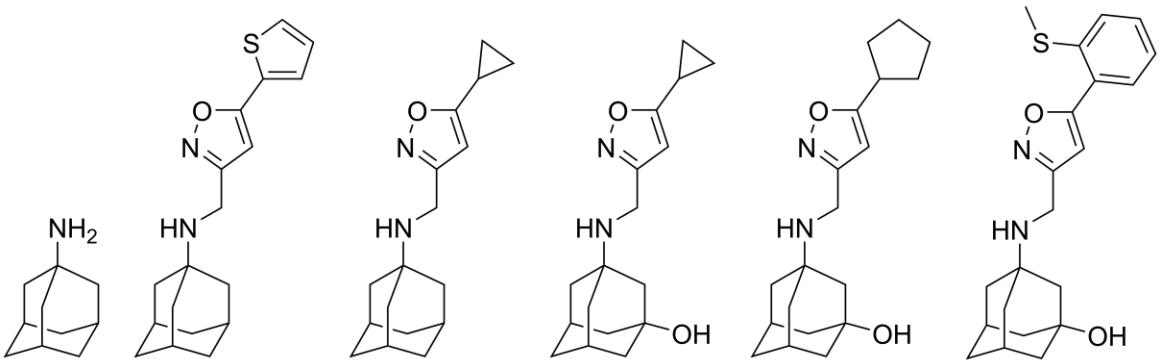

1 2 3 4 5 6

Molecular Pharmacology Fast Forward. Published on June 7, 2019 as DOI: 10.1124/mol.119.116640
This article has not been copyedited and formatted. The final version may differ from this version.

Figure 2

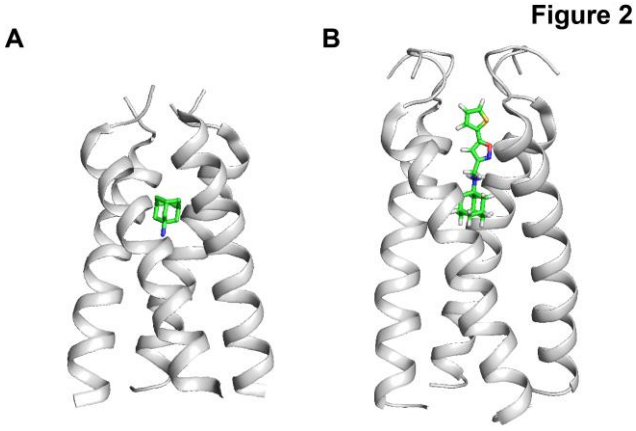

Molecular Pharmacology Fast Forward. Published on June 7, 2019 as DOI: 10.1124/mol.119.116640
This article has not been copyedited and formatted. The final version may differ from this version.

Figure 3

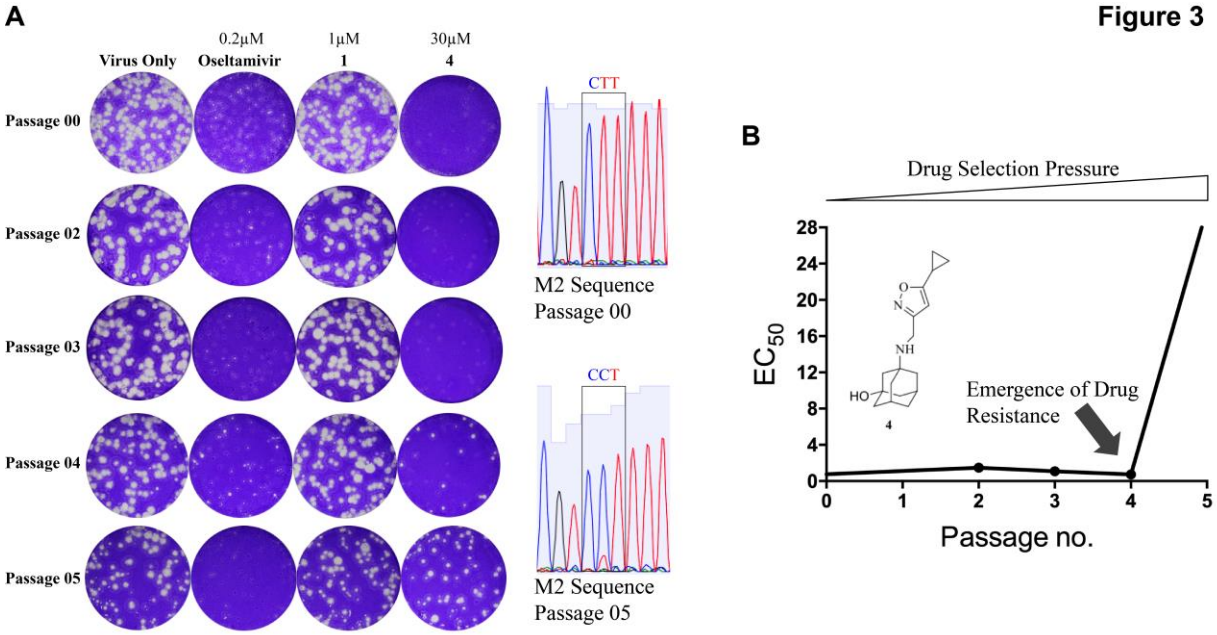

Molecular Pharmacology Fast Forward. Published on June 7, 2019 as DOI: 10.1124/mol.119.116640
This article has not been copyedited and formatted. The final version may differ from this version.

Figure 4

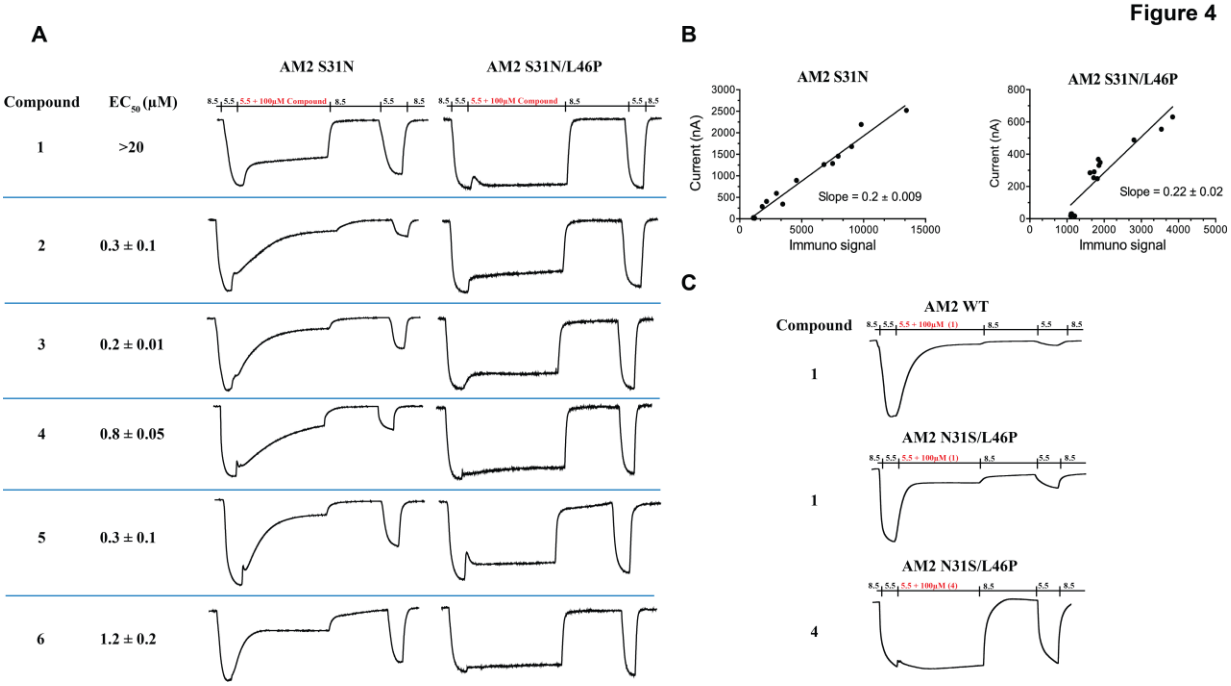

Molecular Pharmacology Fast Forward. Published on June 7, 2019 as DOI: 10.1124/mol.119.116640
This article has not been copyedited and formatted. The final version may differ from this version.

Figure 5

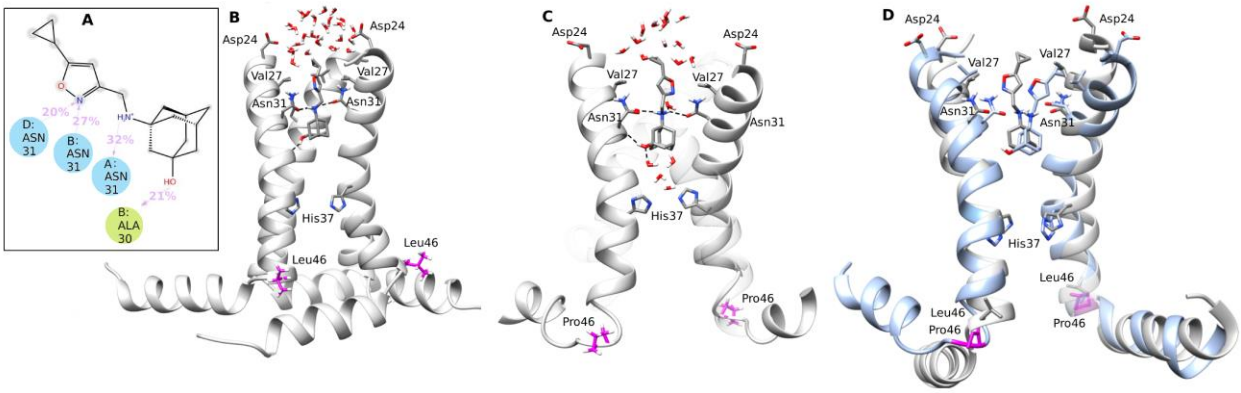

Molecular Pharmacology Fast Forward. Published on June 7, 2019 as DOI: 10.1124/mol.119.116640
This article has not been copyedited and formatted. The final version may differ from this version.

Figure 6